
Towards building a Crowd-Sourced Sky Map

Dustin Lang

McWilliams Center for Cosmology
Carnegie Mellon University
5000 Forbes Ave,
Pittsburgh, PA 15213
dstn@cmu.edu

David W. Hogg

Center for Cosmology and
Particle Physics
New York University
4 Washington Place,
New York, NY 10003
david.hogg@nyu.edu

Bernhard Schölkopf

Max Planck Institute for
Intelligent Systems
Spemannstrasse 38,
72076 Tübingen, Germany
bs@tuebingen.mpg.de

Abstract

We describe a system that builds a high dynamic-range and wide-angle image of the night sky by combining a large set of input images. The method makes use of pixel-rank information in the individual input images to improve a “consensus” pixel rank in the combined image. Because it only makes use of ranks and the complexity of the algorithm is linear in the number of images, the method is useful for large sets of uncalibrated images that might have undergone unknown non-linear tone mapping transformations for visualization or aesthetic reasons. We apply the method to images of the night sky (of unknown provenance) discovered on the Web. The method permits discovery of astronomical objects or features that are not visible in any of the input images taken individually. More importantly, however, it permits scientific exploitation of a huge source of astronomical images that would not be available to astronomical research without our automatic system.

1 Introduction

The Web contains millions of astronomical images in human-viewable formats (eg, jpeg)—the “Astrophotography” group on *flickr* alone has over 68,000 images—and these images contain scientifically valuable information about the night sky. Some of these

images are night-time snapshots, some are carefully rendered visualizations using many images taken by high-quality backyard telescopes. Either way, these images are difficult to use for scientific purposes because they have unknown provenance, and images rendered for human visual consumption are often processed with non-trivial non-linear (and sometimes non-local) transformations. Such transformations are often tone mappings applied to the intensity values (e.g., the gamma transform that is applied to all jpeg images). We also often know nothing (*a priori*) about the point-spread function or vignetting or noise or distortions.

Nonetheless, it remains a holy grail of “internet astrophysics” to learn everything about the night sky that can be learned from the images on the Web; in principle these images may contain a huge amount of information about rare transients, variable stars, and high proper-motion objects. One example of a successful exploitation of Web imaging is the determination of the gravitational orbit of Comet 17P/Holmes using imaging found by Web search (Lang and Hogg, 2011); another is the determination of the impact trajectory of the Chelyabinsk meteoroid from security-camera and other footage (Zuluaga et al., 2013). An interesting new direction—explored here—is to combine the imaging into an all-sky “consensus image” that ideally contains information about the static sky from all images ever taken. This project could take the form of a massive citizen-science project or as a Web-scraping project.

One of the most important capabilities of a consensus image would be its great sensitivity to faint, extended features such as the outskirts of nearby galaxies, nebulae, and—as we explore here—the faint streams of debris that result when two galaxies interact. For extended features, the combined imaging from many small telescopes can be competitive with large telescopes. Indeed, many of the faintest features known

Appearing in Proceedings of the 17th International Conference on Artificial Intelligence and Statistics (AISTATS) 2014, Reykjavik, Iceland. JMLR: W&CP volume 33. Copyright 2014 by the authors.

in nearby galaxies were found with telescopes 16 to 50 cm in diameter (Martínez-Delgado et al., 2008, 2009, 2010).

The key problem we face is extraction of scientifically valuable information from the images without detailed knowledge of image provenance or processing. In particular, we want to combine the information from many images to produce highly informative, high dynamic-range images that go much deeper than any individual contributing image, and we want to do this without having to infer the (possibly highly nonlinear) processing that has been applied to each individual image, each of which has been wrecked in its own loving way by its creator.

The problem we are tackling is different than related problems because we are truly photon-limited: we want to increase the effective exposure time (sensitivity) of our consensus image by combining the exposure time of a large number of independent input images. In astronomical images, it is nearly always the case that if we had additional exposure time, we would detect more (faint) objects, or more clearly resolve faint extended features. In typical *high dynamic range* imaging problems known from computer vision, in contrast, the issue is to capture and represent (perhaps artistically) an increased range of contrasts; it is assumed that it is easy to *capture* the image with the longest exposure time in a single exposure, and typically only a few exposure times are required to capture a satisfactory dynamic range. In *lucky imaging* problems (Law et al., 2006; Joshi and Cohen, 2010), the goal is typically to achieve the highest possible *resolution*; sensitivity or signal-to-noise is secondary. In *panorama stitching* (Brown and Lowe, 2007; Levin et al., 2004), the primary goal is to increase the areal coverage of the image; a single image is usually deemed sufficient to represent the scene in a given region, and the challenge is to register and blend the images to produce seamless mosaics. In *photo-tourism* (Snavely et al., 2006; Agarwal et al., 2009), the multiple images provide different viewpoints and levels of detail; again, a single image is typically sufficient to capture the required level of detail or dynamic range.

Our problem setting also differs from typical astronomical image processing for scientific purposes. Usually, great care is taken to calibrate the detector so that pixel values can be mapped back to intensity (photon counts) linearly. Combining multiple images is then a straightforward matter of registering the images and producing a weighted sum. At the faint end, the sensitivity of typical astronomical images is limited by noise from reading out the detector and from atmospheric and other background emission (with Poisson noise) competing with the signal of interest. Increasing the

exposure time thus increases the signal-to-noise ratio. The Hubble Ultra-Deep Field processed images, for example, sum hundreds of exposures in each of four bands in order to increase the sensitivity (depth) to detect extremely faint objects. In our problem setting, we cannot assume linearly calibrated images, so a more elaborate method of combining images is required.

More generally, this project connects to other comprehensive projects that hope to make use of large, heterogeneous collections of data: Data can only be used simultaneously if it can be calibrated onto some kind of common reference system. The rank statistics used here provide a robust basis for this. More specifically, in astrophysics there are no agreed-upon or generally useful robust methods for combining heterogeneously processed images from disparate sources. Images from multiple telescopes are rarely combined, even when calibration is well understood; essentially never when it is ill understood. Historical astronomical image collections, for example, contain sky coverage equivalent to the entire sky imaged hundreds or even thousands of times over; yet they haven't been combined into any kind of master image as of today.

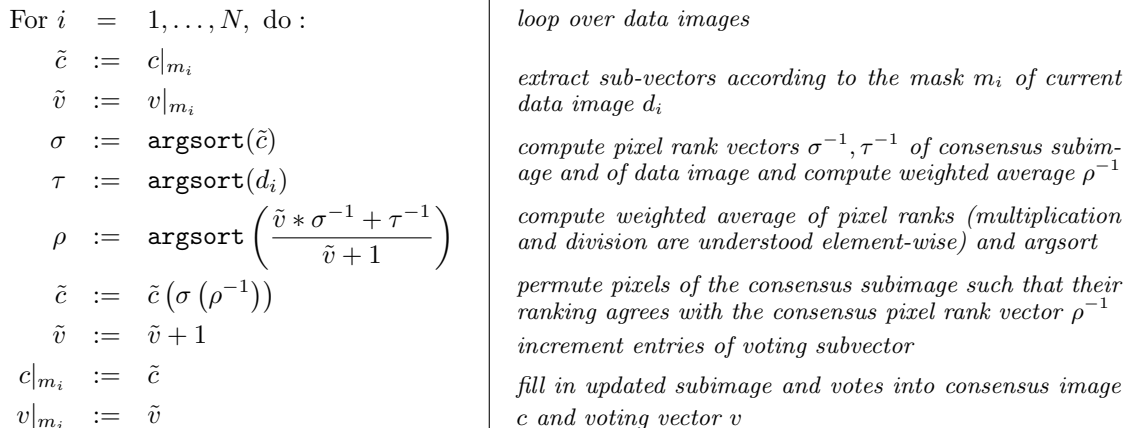
2 Method

We have N images i that have been registered and re-sampled to the same pixel grid. Each image contains pixel values (“data”) d_i , where d_i can be thought of as a vector as long as the number of pixels in the image. The intensity field I (energy per time per solid angle per logarithmic wavelength interval) generates the data d_i only after convolution with the appropriate point-spread function, transformation to the relevant pixel grid, and sampling. We represent this transformation as a linear operator H_i acting on the intensity field. The linearly transformed intensity field $H_i \cdot I$ is transformed non-linearly through a monotonically increasing function $f_i(\cdot)$ to “data values” and noise e_i is added to make the observed data:

$$d_i = f_i(H_i \cdot I) + e_i \quad (1)$$

In reality, the noise is probably not precisely additive. The non-linear mapping f_i includes detector effects such as saturation, as well as post-processing (gamma correction, white balance, etc), performed either in the camera or in photo-editing software. We assume that f_i is monotonically increasing; If we don't have further information about f_i , the absolute values of d_i do not carry useful information. However, *ranks* among observed values can be exploited.

Combining ranks from a set of multiple images is a problem of *rank aggregation*. This problem is usually

Figure 1: Proposed *Enhance* algorithm.

formalized as finding a permutation which minimizes the Kendall-tau distance to the input rankings (Kemeny rank aggregation), in which case it is known to be NP-hard (for an overview, see Schalekamp and van Zuylen (2009)). Most methods either specialize on aggregating many short ranked lists (e.g., for voting), or few long lists (e.g., for meta-search engines, or certain bioinformatics applications). One way to build efficient heuristic methods is to use a *positional* approach, i.e., to seek a permutation in which the position of each element is “close to the average position” of the element in the input lists (Schalekamp and van Zuylen, 2009). We will propose such a method for our problem, fully aware that this does not solve the exact rank aggregation problem. Indeed, for the setting of few long lists, a common approach is to use Markov chain based heuristics (for a discussion, see Lin (2010)). Our setting contains long lists (with millions of entries) and a potentially large number of such lists.

Let c be the *consensus* image that we are trying to compute, containing P pixels. This may be a rectangular image of a certain area of the sky, or an array of possibly non-rectangular pixels uniformly covering the celestial sphere. Since we are only concerned with pixel ranks, we initialize it as a vector whose elements form a random permutation of $\{1, \dots, P\}$. Our algorithm will ensure that after each update step, the entries of c are again a permutation of $\{1, \dots, P\}$, aggregating the information about the pixel ranks as presented in the *observed images* or *data* d_i . The data will usually cover a proper sub-field of c only, modeled by a binary *mask* vector m_i whose entry is 1 if and only if the corresponding entry is covered by d_i . The data image d_i will update the consensus image c only according to its footprint, i.e., in the restriction of c to the mask m_i , denoted $c|_{m_i}$ (i.e., the sub-image consisting of those pixels where $m_i = 1$).

Along with the consensus image c , we keep a vector of *votes* v , initialized to $(0, \dots, 0) \in \mathbf{R}^P$. For each pixel of c , the corresponding value in v records how many data images have contributed to it so far by voting for its rank.

Let **argsort** be an $O(n \log n)$ function that, given a vector d of length n , returns a permutation σ so that $d(\sigma)$ is sorted in non-decreasing order.¹ The inverse permutation σ^{-1} is a function that maps an index p in the vector d to the *rank* of its entry d_p among the set of all entries.

The proposed *Enhance* algorithm proceeds as shown in Figure 1. Let us discuss some details and properties of the method.

Tied ranks. Due to clipping and quantization, a data image d_i often has sets of identical entries. In this case, there are several permutations τ sorting it. In practice, we average the corresponding ranks τ^{-1} to get what is called the *tied rank*; with some abuse of notation, we refer to it as τ^{-1} .

Invariant Histogram. Since the pixel values in the consensus image are only permuted, the final image has the same pixel histogram as its initialization. It can easily be post-processed to make a pixel histogram that is in accord with prior expectations, for instance taking into account models of sensor noise, sky background, star brightness distributions, point spread functions, etc; or histogram-matched to a given image.

Above, we initialized c to a random permutation of $\{1, \dots, P\}$. Other initializations are possible as well, including

¹ $d(\sigma)$ is a composition of σ and d where the vector d is thought of as a function on its index set

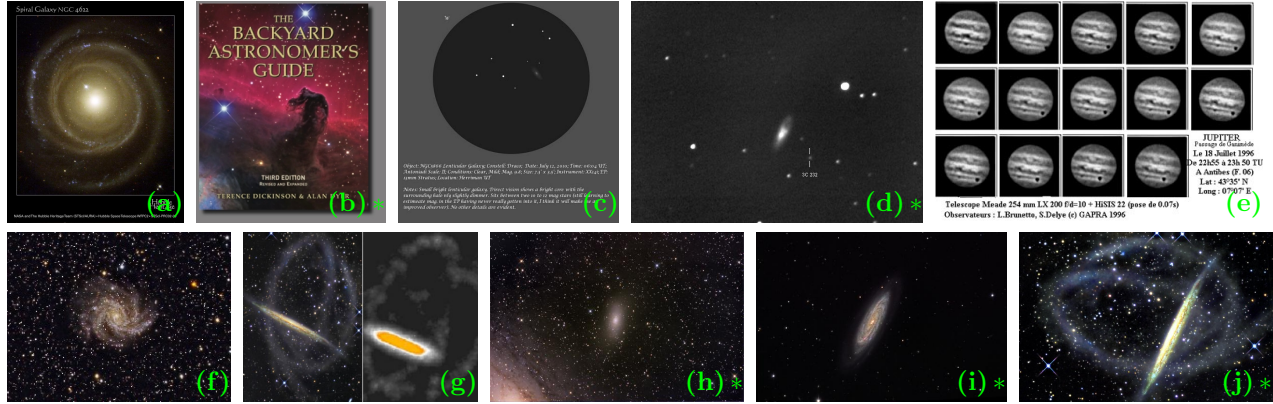


Figure 2: Example images found through our Web search for images of NGC 5907. Images that were successfully calibrated by *Astrometry.net* are marked with *. Notice that for this rather distinctive search term, most images are actually astronomical in nature but relatively few are actually images of NGC 5907—only (g) and (j) here, and roughly 450 of the 2000 images resulting from our Web search.

- a random image with a specified histogram (which will remain invariant, since the entries of c only get permuted by the algorithm),
- a ‘current best guess’ image, for instance based on existing sky maps, or a previous run of the algorithm.

Convergence. The choice of the voting weights ensures that for each pixel, each data image that contributed to it will have had the same relative weight in the algorithm’s averaging step. This does not, however, imply that the algorithm is invariant to the ordering of the images: As images are combined, the total weight vector \tilde{v} accumulates. Eventually, the total weight becomes large enough that new images simply do not have enough influence to change the ordering of the pixels in the consensus image. The maximal image size is P pixels, hence the maximal rank difference that can be observed in an image d_i is $P - 1$; this ranking will come with a weight of 1. The current consensus image, however, will receive weight v . Once all entries of v are at least P , i.e., once every pixel has been covered by at least P data images, the averaging step can no longer change the ranking of the consensus image, and the algorithm has converged, at the expense of any influence of late-arriving input images.

In our application, we are far from this happening (P is of order 10^6 , and we are nowhere near to having a comparable number of images at this point). Nevertheless, one can think of strategies to avoid this:

- Use mini-batches of image that are combined to a separate consensus image with a nontrivial voting vector, which can then be combined with the current consensus image (using a straightforward generalization of our voting formula).

- Assign non-binary weights to data images, to ensure that rankings are considered more reliable where the pixel values were different, and the rankings thus reliable. For instance, if 10% of the pixels have exactly the same value (due to discretization or clamping, say), then the ranks of those pixels are uncertain at $\sim 10\%$; if we assume a constant per-pixel error standard deviation in the input images, then the rank error is the per-pixel error times the derivative of the ranking function, ie, the normalized histogram value. Given Gaussian noise this would suggest a per-pixel weighting of $1/h(d_i)^2$, where h is the histogram. This would dramatically increase the maximal possible influence of individual images, delaying the convergence.

Astrometry.net Before combining the images, we need to recognize them (as images of the night sky) and register them to a common celestial coordinate system. These tasks are performed by a system, *Astrometry.net*, that has been described in the astronomical literature (Lang et al., 2010), but not in the machine learning or statistics literature. *Astrometry.net* image recognition and calibration proceeds in three stages:

In the star-measuring phase, a rough noise estimate is made in the input image by a median-absolute-difference analysis and statistically significant peaks are identified as possible “stars”. Each star is given a measured centroid and brightness by a fit of a quadratic function to a pixel patch centered on its peak pixel in the image.

In the geometric-hashing phase, sets of four stars are considered sequentially (and exhaustively in an order-

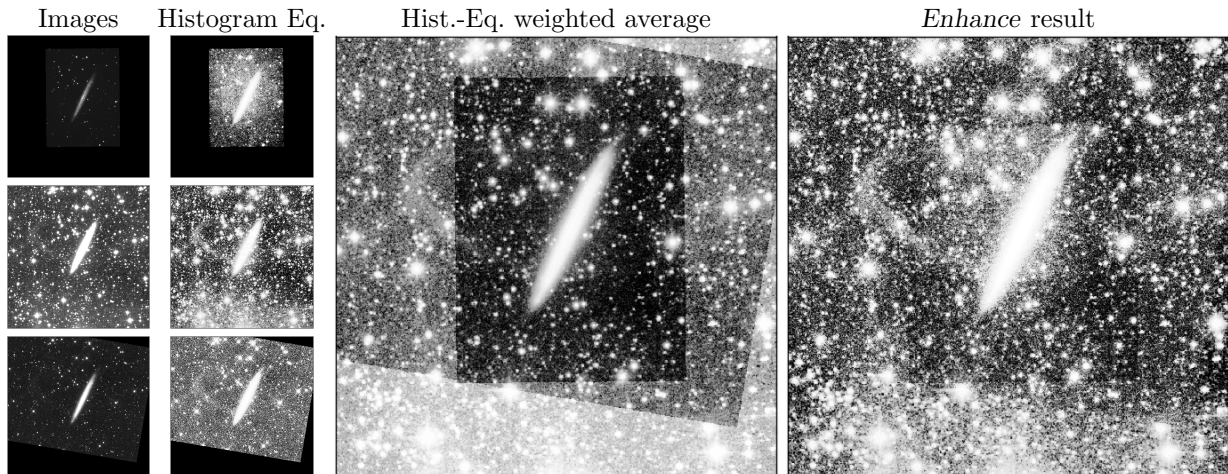


Figure 3: Four example images from the NGC 5907 collection, chosen to show very different dynamic range and pre-processing. **Left column:** Input images (resampled to the common pixel grid). The top two images have very low saturation (very few pixels with the maximum value); the bottom two images have high saturation. **Middle column:** Histogram-equalized input images. **Top-right:** The histogram-equalized average of the input images; image borders are clearly visible and the resulting image does not clearly show more dynamic range than the inputs. **Bottom-right:** Result of running the *Enhance* algorithm. The input image edges are less prominent, and the looping streamer feature as well as the details in the core of the galaxy are visible due to the enhanced dynamic range.

ing based on star brightnesses, limited only by CPU time). For each set of four stars, a geometric hash is computed that is invariant to translation, rotation, and scale. This hash is looked up in an index of hashes of known four-star asterisms (combinations of stars), with a finite tolerance to account for measurement noise, small camera distortions, and stellar proper motions. Any match of a four-star hash with an indexed hash creates a “proposal” for the mapping between image coordinates and celestial coordinates. The pre-computed index of four-star hashes is designed to cover the entire sky densely, not over-use individual stars (which might be noisy or variable or wrong in the input catalogs), and make use of stars that are likely to be co-visible in normal images.

In the decision phase, every proposal about the coordinate mapping generated in the hashing phase is used to make predictions about the positions of *other* stars in the image (other than the four used to make the hash), based on the positions of known stars. A robust likelihood for the proposal is computed, permitting there to be known stars not detected in the input image, and detected stars in the input image that are not known. The posterior probability for the proposal and a null hypothesis (that the hash alignment has been found by chance) are compared, to make a decision in the context of Bayesian decision theory with a well-defined utility function. The utility function is designed to be conservative (that is, reject a match unless there is overwhelming support for it).

After a finite amount of CPU time, the system either returns a failure or else the full mapping between image coordinates and celestial coordinates. This mapping is delivered in standards-compliant astronomical format (FITS WCS). In detail, it delivers a full polynomial model of the camera distortions away from a tangent-plane projection. In particular, for the purposes of this project, the output of *Astrometry.net* includes the celestial footprint of the image and the precise transformation from pixel position to celestial position for every pixel in the input image, thus solving the problem of registering the images to a common pixel grid.

3 Experiments

Our method is defined for collections of images of a fixed or near-fixed scene from a near-fixed viewpoint. The images must be registered and resampled onto a common pixel grid, with associated mask images showing the registered image footprint on the reference “canvas”. We obtained two example image collections of extended astronomical objects from the Web, one for the galaxy NGC 5907 and one for the interacting pair of galaxies Messier 51a and 51b. In the case of NGC 5907, the goal was to use (shallow, non-scientific) images available on the Web to rediscover or confirm astrophysically important but very faint (low surface-brightness) features discovered in the outskirts of the galaxy (Martínez-Delgado et al., 2008). We



Figure 4: *Top left*: deep image from Martínez-Delgado et al. (2008), showing a faint stellar stream. This is a visualization of the deepest image ever taken of NGC 5907. *Top right*: example images from our set of 298 images, obtained by a Web search for NGC 5907 (see Figure 2), and manually removing images that show the stellar stream visible in the deep image. *Bottom, left to right*: results obtained by our algorithm, tone-mapped to have the same histogram as the deep image: after one run through the image set; after one run using a different permutation of the image set; and ten runs through the image set. While the algorithm is not strictly invariant to image reordering, the results are visually quite similar. Also, it is noteworthy that one pass through the dataset gives very good results, showing the faint stellar stream visible in the deep image, which required over 11 hours of exposure time on a 0.5-meter telescope.

chose the first target (NGC 5907) since a high-quality “ground truth” image is available, and the second target (Messier 51) because we knew a large number of images would be available.

We generated the image collections using the “image search” APIs of *flickr*, *Bing*, and *Google*. For the first target—NGC 5907—we used the search terms “NGC5907” and “NGC 5907”. We retrieved as many results as the APIs would allow (4000 for *flickr*, 1000 for *Bing*, and 100 for *Google*), and repeated the search with different filters on the image size in order to get the largest possible set of results. Examples of the images produced by this search are shown in Figure 2.

Many images returned by the Web search services were not images of the sky, or else not useful images, or else images of the sky but not including the target; attempted recognition with the *Astrometry.net* system filtered these out. In Figure 2 we have marked the images that were recognized as images of the sky. We also filtered the images by hand to remove images with very prominent labeling or overplotted diagrams or text decoration, and removed the highest-quality images (taken by Martínez-Delgado et al. (2008), or derived or reprocessed from those images) that individually show the low intensity features of greatest

interest. We believe both removals could have been performed automatically with objective operations on the pairwise rank statistics, but implementation was beyond the deadline-limited scope of this project.

The Web search services returned a total of 2034 image URLs, of which 1967 were retrievable and had unique contents, and 1817 were jpeg images. Of these, 405 were recognized as images of the night sky overlapping our target region near NGC 5907. Of these, 48 were images from Martínez-Delgado et al. (2008) or reprocessings of those images, and we marked an additional 59 images as having excessive annotations or markings. The experiments below use the remaining 298 pixel-aligned images of NGC 5907.

A reference 900×900 pixel grid (canvas) in a tangent-plane projection of the sky 30×30 arcmin² in solid angle (roughly the area of the full moon) was generated, centered on the fiducial celestial position of NGC 5907 (RA, Dec = 229, 56.3 degrees J2000). The *Astrometry.net*-recognized images—which in recognition are also given standards-compliant celestial-coordinate-system meta-data—were resampled by nearest-neighbor resampling onto the reference grid. Many of the input images did not fully cover the reference image canvas; we produced a mask indicating



Figure 5: Example images from the M51 collection (resampled to the reference grid), and the result of the *Enhance* algorithm acting on all 2066 images in the collection; *Bottom left*: Histogram-equalized consensus image; *Bottom right*: Consensus image, tone-mapped to the second image in the top row. Notice the faint extended structures around both galaxies: this is the debris resulting from their strong gravitational interaction.

which reference pixels were covered by each input image.

For the first experiment with the NGC 5907 data, we chose four images with different dynamic range (shown in Figure 3). We performed a weighted average of these images, weighted by their mask vectors. We also combined them according to the *Enhance* algorithm given in the Method Section. The reference image was initialized with the histogram-equalized average image. The results are shown in Figure 3. *Enhance* combines the images to produce an image with high overall dynamic range.

For the second experiment, we ran the *Enhance* algorithm on all 298 images in the collection, initializing with the mean image. We ran the red, green, and blue color channels separately. The results are shown in Figure 4.

We compute an approximate measure of the Kendall tau rank-correlation coefficient between the *Enhance* consensus image and one of the high-quality deep images of NGC 5907 that we removed from the input image set (with the manual filtering). We compare

this to the Kendall tau for a simple mask-weighted average of the input images and the same deep image. The *Enhance* output gets Kendall tau of 0.355 and the weighted average 0.183, demonstrating that *Enhance* produces a consensus image much closer to our proxy for “ground truth”. Furthermore, the mean inter-image Kendall tau between pairs of input images is 0.165 whereas the mean Kendall tau between input images and the consensus image produced by *Enhance* is 0.249, demonstrating that the consensus is good.

For the third experiment, the Messier 51 image collection was used. Analysis was identical, except that the search terms included several aliases for the galaxy: “M 51”, “Messier 51”, “Whirlpool Galaxy”, “M 51a”, “M 51b”, “NGC 5195”, “NGC 5194”, “UGC 8494”, “PGC 4741”, “Arp 85”, plus the same phrases without spaces. The reference grid was centered on RA,Dec = (202.5, 47.22) degrees J2000, with 1080×1080 pixels and an area of 18×18 arcmin². The search yielded 13,472 URLs, of which 12,793 were unique retrievable files, 11,709 were jpeg images, 2072 were recognized by *Astrometry.net*, and 2066 overlapped our region of interest. (We instructed *Astrometry.net* to search only

in a small region around M51.) The results, which took about 40 minutes on a single processor, are shown in Figure 5.

4 Discussion

We have proposed a system that can automatically combine uncalibrated, processed night-sky images to produce high quality, high dynamic-range images covering wider fields. The consensus images output by *Enhance* shown in Figures 4 and 5 reveal very low-surface brightness tidally disrupted features from violent galaxy–galaxy interactions between subcomponents of each system. These faint features are of great astrophysical importance—they permit (in principle) measurement of the ages, mass ratios, and orbital configurations of recent merger events—and yet some of them are not clearly visible in any of the input images. *Enhance* creates opportunities for new astronomical discoveries.

Our method scales linearly in the number of images, making it applicable to the large (and increasing) number of astronomical images available. For each update step, the time complexity is $n \log n$ (due to the sorting algorithm) in the image size n of the new image being added (and independent of the consensus image), taking a few seconds on a laptop for a 3 Megapixel image in matlab. The method can thus be applied to internet-scale problems.

We have set up a Web site that allows users to submit images for combination into an Open-Source Sky Map.² The system keeps an overall sky map (in celestial coordinates), whose brightness ranks are initialized as a random permutation, as described above. Every time an image is submitted, the system recognizes and calibrates the image with *Astrometry.net* and merges its rank information into our overall rank map as described. We make use of the astronomical-standard HealPix pixelization of the sky for the all-sky map (Górski et al., 2002). In return, users receive annotated versions of their images, as well as a histogram-matched version of the corresponding part of the current state of the map. The former allows the identification of known astronomical objects, while the latter is informative with respect to any differences to the present images, helpful for identifying transient events as well as noticing any issues with calibration or instrumentation. A limitation for these applications of the current system, and a promising direction for future research, is the inclusion of point spread function modeling.

One key value of pixel rank representations of images is

that they permit identification of non-identical input images that nonetheless were created from the same original source data (telescope or camera images). In principle we should identify these duplicates and use only one copy. However, the inclusion of duplicates or images related by having common raw-data origins does not have a large negative impact on the *Enhance* output; these images just end up having higher overall influence on the consensus ranks in the final output.

The specific *Enhance* algorithm given here works on static two-dimensional scenes. That is, it cannot be applied to time-variable scenes or three-dimensional scenes with multiple camera viewpoints without substantial modification. However, there are many natural-image applications for which the assumptions of *Enhance* apply. Shots of famous landmarks from other famous landmarks could be used (for example the Brooklyn Bridge viewed from the Empire State Building Observation Deck). Images taken in different weather conditions with different cameras, processed differently could be registered and then combined with *Enhance*.

Finally, one scientifically very important application for *Enhance* is in the analysis of historical photographic plate data. Astronomical data in photographic (glass) plate form dates back to the 1880s or earlier, and the Harvard Plate Archives alone contain half a million plates, covering the sky hundreds of times over. Different emulsions, different exposures, different developing, and different pre-exposure plate treatment (“hypering”) lead to different non-linear responses of emulsion density to incident intensity. These valuable plate images can be compared and combined with pixel-rank statistics without a full treatment of all non-linear effects. *Enhance* could have a large impact on historical astronomy and astrophotography.

References

- S. Agarwal, N. Snavely, I. Simon, S. M. Seitz, and R. Szeliski. Building rome in a day. In *International Conference on Computer Vision*, 2009.
- M. Brown and D. G. Lowe. Automatic panoramic image stitching using invariant features,. *International Journal of Computer Vision*, 74(1):59–73, 2007.
- K. M. Górski, A. J. Banday, E. Hivon, and B. D. Wandelt. HEALPix — a Framework for High Resolution, Fast Analysis on the Sphere. In D. A. Bohlender, D. Durand, and T. H. Handley, editors, *Astronomical Data Analysis Software and Systems XI*, volume 281 of *Astronomical Society of the Pacific Conference Series*, pages 107–+, 2002.
- N. Joshi and M. F. Cohen. Seeing Mt. Rainier: Lucky Imaging for Multi-Image Denoising, Sharp-

²<http://nova.astrometry.net>

- ening, and Haze Removal. *International Conference on Computational Photography*, 2010.
- D. Lang and D. W. Hogg. Searching for comets on the World Wide Web: The orbit of 17P/Holmes from the behavior of photographers. *The Astronomical Journal*, 144:46, 2011. arXiv:1103.6038.
- D. Lang, D. W. Hogg, K. Mierle, M. Blanton, and S. Roweis. Astrometry.net: Blind astrometric calibration of arbitrary astronomical images. *The Astronomical Journal*, 137:1782–2800, 2010. arXiv:0910.2233.
- N. M. Law, C. D. Mackay, and J. E. Baldwin. Lucky imaging: high angular resolution imaging in the visible from the ground. *Astronomy & Astrophysics*, 446:739–745, 2006.
- A. Levin, A. Zomet, S. Peleg, and Y. Weiss. Seamless image stitching in the gradient domain. In *Proceedings of the European Conference on Computer Vision*, 2004.
- S. Lin. Rank aggregation methods. *Wiley Interdisciplinary Reviews: Computational Statistics*, 2:555–570, 2010.
- D. Martínez-Delgado, J. Peñarrubia, R. J. Gabany, I. Trujillo, S. R. Majewski, and M. Pohlen. The Ghost of a Dwarf Galaxy: Fossils of the Hierarchical Formation of the Nearby Spiral Galaxy NGC 5907. *The Astrophysical Journal*, 689:184–193, December 2008.
- D. Martínez-Delgado, M. Pohlen, R. J. Gabany, S. R. Majewski, J. Peñarrubia, and C. Palma. Discovery of a Giant Stellar Tidal Stream Around The Disk Galaxy NGC 4013. *The Astrophysical Journal*, 692:955–963, February 2009.
- D. Martínez-Delgado, R. J. Gabany, K. Crawford, S. Zibetti, S. R. Majewski, H.-W. Rix, J. Fliri, J. A. Carballo-Bello, D. C. Bardalez-Gagliuffi, J. Peñarrubia, T. S. Chonis, B. Madore, I. Trujillo, M. Schirmer, and D. A. McDavid. Stellar Tidal Streams in Spiral Galaxies of the Local Volume: A Pilot Survey with Modest Aperture Telescopes. *The Astronomical Journal*, 140:962–967, October 2010.
- F. Schalekamp and A. van Zuylen. Rank aggregation: Together we’re strong. In *Algorithm Engineering and Experimentation*, pages 38–51, 2009.
- N. Snavely, S. M. Seitz, and R. Szeliski. Photo tourism: Exploring photo collections in 3d. In *SIGGRAPH Conference Proceedings*, pages 835–846, New York, NY, USA, 2006. ACM Press.
- J. I. Zuluaga, I. Ferrin, and S. Geens. The orbit of the Chelyabinsk event impactor as reconstructed from amateur and public footage. <http://arxiv.org/abs/1303.1796>, 2013.